The Astrophysical Journal Letters, 721:L58–L61, 2010 September 20 doi:10.1088/2041-8205/721/1/L58

THE ELECTRICAL CURRENT DENSITY VECTOR IN THE INNER PENUMBRA OF A SUNSPOT

K. G. Puschmann[1,2], B. Ruiz Cobo[1,2], and V. Martínez Pillet[1]
[1] Instituto de Astrofísica de Canarias (IAC), E-38200 La Laguna, Tenerife, Spain; kgp@iac.es, brc@iac.es, vmp@.iac.es
[2] Departamento de Astrofísica, Universidad de La Laguna (ULL), E-38205 La Laguna, Tenerife, Spain
Received 2010 July 15; accepted 2010 August 10; published 2010 September 1

ABSTRACT

We determine the entire electrical current density vector in a geometrical three-dimensional volume of the inner penumbra of a sunspot from an inversion of spectropolarimetric data obtained with *Hinode*/SP. Significant currents are seen to wrap around the hotter, more elevated regions with lower and more horizontal magnetic fields that harbor strong upflows and radial outflows (the intraspines). The horizontal component of the current density vector is 3–4 times larger than the vertical; nearly all previous studies only obtain the vertical component J_z, thus strongly underestimating the current density. The current density $\vec{J}$ and the magnetic field $\vec{B}$ form an angle of about 20°. The plasma β at the 0 km level is larger than 1 in the intraspines and is one order of magnitude lower in the background component of the penumbra (spines). At the 200 km level, the plasma β is below 0.3, nearly everywhere. The plasma β surface as well as the surface optical depth unity is very corrugated. At the borders of intraspines and inside, $\vec{B}$ is not force-free at deeper layers and nearly force-free at the top layers. The magnetic field of the spines is close to being potential everywhere. The dissipated ohmic energy is five orders of magnitudes smaller than the solar energy flux and thus negligible for the energy balance of the penumbra.

Key words: methods: numerical – methods: observational – Sun: magnetic topology – sunspots – techniques: polarimetric

1. INTRODUCTION

The study of the stability or dynamics of penumbral filaments requires the knowledge of the Lorentz force, i.e., an accurate determination of the electrical current density vector $\vec{J}$ and the magnetic field vector $\vec{B}$. The estimation of the energy budget dissipated by electrical currents obviously requires the determination of $\vec{J}$. However, it is not trivial to reliably derive the electrical currents from observational data. Previous attempts were aimed almost exclusively at the determination of only the vertical component J_z with different degrees of sophistication in the analysis of the data. The bulk of such studies was based on magnetograms (Deloach et al. 1984; Hagyard 1988; Hofmann et al. 1988, 1989; Canfield et al. 1992; de la Beaujardiere et al. 1993; Leka et al. 1993; Metcalf et al. 1994; van Driel-Gesztelyi et al. 1994; Wang et al. 1994; Zhang & Wang 1994; Gary & Demoulin 1995; Li et al. 1997; Gao et al. 2008). More accurate estimates of J_z stem from state-of-the-art spectropolarimetric observations and the application of inversion techniques. In the case of Milne–Eddington (ME) inversions (e.g., Skumanich & Lites 1987; Lagg et al. 2004), $\vec{B}$ is obtained at an average optical depth. Among the recent works calculating J_z under ME approximation, one finds Shimizu et al. (2009), Venkatakrishnan & Tiwari (2009), and Li et al. (2009). An alternative determination of J_z is obtained by Balthasar (2006), Jurcák et al. (2006), and Balthasar & Gömöry (2008) employing Stokes inversion based on response functions (SIR; Ruiz Cobo & del Toro Iniesta 1992), which delivers the stratification of $\vec{B}$ in an optical depth scale.

There have been several attempts to obtain $J_{\rm hor}$, the modulus of the horizontal component of $\vec{J}$, imposing approximations to the magnetic field distribution: Ji et al. (2003) and Georgoulis & LaBonte (2004) obtain a lower limit of $J_{\rm hor}$ assuming a field-free configuration; Pevtsov & Peregud (1990) derive $J_{\rm hor}$ imposing cylindrical symmetry of $\vec{B}$ in a sunspot. Without making any hypothesis on $\vec{B}$, the determination of the three components of $\vec{J}$ requires knowledge of the entire magnetic field vector in a geometrical three-dimensional (3D) volume, i.e., the determination of a *geometrical* height scale is mandatory. While commonly in the quiet Sun the transformation from an optical depth scale to geometrical heights is done by assuming hydrostatic equilibrium (see, e.g., Puschmann et al. 2005), this is not justified in the magnetized penumbra. In this case, the force balance must include magnetic forces, which requires one to calculate the horizontal and vertical spatial derivatives of $\vec{B}$. The first attempt to *empirically* derive 3D vector currents was done by Socas-Navarro (2005), who determined a geometrical height scale (following Sánchez Almeida 2005) by imposing equal total pressure between adjacent pixels, although neglecting the magnetic tension in the Lorentz force.

For an accurate determination of $\vec{J}$ in this Letter, we take advantage of the 3D geometrical model of a section of the inner penumbra of a sunspot described in Puschmann et al. (2010, hereafter, Paper I). We use observations of the active region AR 10953 near solar disk center obtained on 2007 May 1 with the *Hinode*/SP. The inner, centerside, penumbral area under study was located at a heliocentric angle $\theta = 4\overset{\circ}{.}63$. To derive the physical parameters of the solar atmosphere as a function of continuum optical depth, the SIR inversion code was applied on the data set. The 3D geometrical model was derived by means of a genetic algorithm that minimized the divergence of the magnetic field vector and the deviations from static equilibrium considering pressure gradients, gravity, and the Lorentz force. For a detailed description, we refer to Paper I.

2. RESULTS AND DISCUSSION

The current density vector $\vec{J} = (\nabla \times \vec{B})/\mu_0$ has been calculated for each pixel in the field of view analyzed in Paper I at geometrical height layers between 0 and 200 km, i.e., in a volume of (4.2 Mm × 5.6 Mm × 0.2 Mm) in the inner penumbra

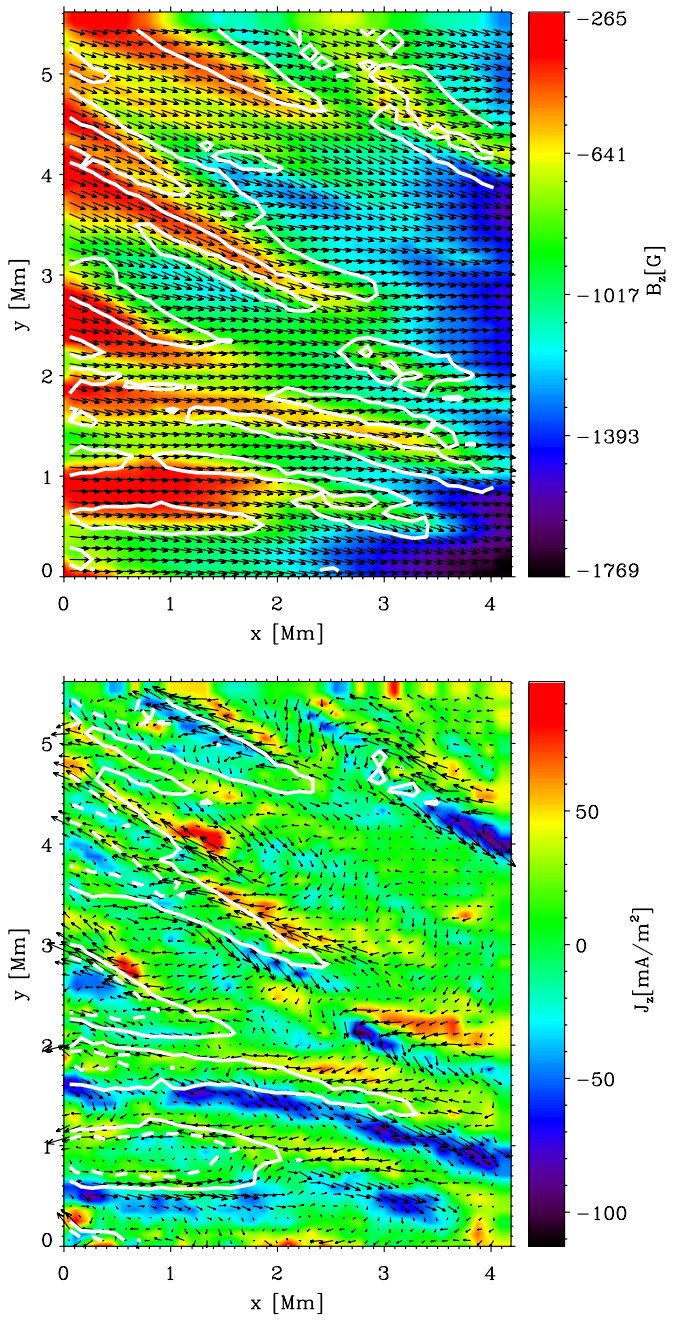

Figure 1. Upper panel: B_z (in color) and $\vec{B}_{\rm hor}$ (arrows) at $z = 200$ km. The size of the arrows ranges from 1220 to 1900 G. The contour lines enclose areas with $J > 120$ mA m^{-2}. Lower panel: J_z (in color) and $\vec{J}_{\rm hor}$ (arrows) at $z = 200$ km. The size of the arrows ranges from 1 to 365 mA m^{-2}. The contour lines correspond to B_z equal to -650 G (solid lines) and to -450 G (dashed lines).

of a sunspot placed close to the disk center. We decompose $\vec{B} = B_z\vec{e}_z + \vec{B}_{\rm hor}$, where $\vec{e}_z$ denotes the unit vector in the vertical direction. In a similar way, we write $\vec{J} = J_z\vec{e}_z + \vec{J}_{\rm hor}$. Throughout the paper, B, $B_{\rm hor}$, J, and $J_{\rm hor}$ will denote the modulus of the corresponding vectors. The upper panel of Figure 1 shows B_z (colored background) and $\vec{B}_{\rm hor}$ (black arrows) at the top layer (200 km). Areas in red color correspond to regions with lower and more horizontal magnetic field (intraspines; Lites et al. 1993) which are hotter, elevated, and harbor strong upflows and radial outflows (see Paper I). These regions can be interpreted as the embedded nearly horizontal flux tubes of the uncombed scenario (see, e.g., Solanki & Montavon 1993; Schlichenmaier et al. 1998a, 1998b; Martínez Pillet 2000; Borrero & Solanki 2010, and references therein). We will refer to regions with a more vertical and intense magnetic field as spines (they correspond to the background component in the uncombed scenario). White contour lines enclose areas with significant J values (larger than 120 mA m^{-2}), located predominantly along the borders of the intraspines. The lower panel of Figure 1 shows J_z (colored background) and $\vec{J}_{\rm hor}$ (black arrows). White contour lines correspond to B_z values equal to -450 (solid) and -650 G (dashed), respectively. The electrical currents wrap around the nearly horizontal flux tubes (intraspines): for the majority of the intraspines, J_z shows positive values at the upper (larger Y-coordinate) borders of the filaments and negative values at the lower borders. The orientation of the black arrows indicates that the currents circumvent the flux tubes in most cases.

In the left panel of Figure 2, we plot the histogram of J_z evaluated at the top layer (200 km) in black. To check the significance of the results, we evaluate a simulated electrical current density distribution $\vec{J}_{\rm err}$. The random vector field $\vec{J}_{\rm err}$ deviates from zero only by Gaussian noise with a σ equal to the estimated error at each pixel for each component of $\vec{J}$; σ was obtained from an error propagation of the uncertainties of $\vec{B}$. The histogram of $J_{\rm err,z}$ is represented in red. Frequently, the z-component of the current density is evaluated from the results of ME inversions; to determine the reliability of such results we performed an ME analysis of our data set, and we calculated the vertical current density $J_{z,\rm ME}$. The histogram of $J_{z,\rm ME}$ is plotted in blue in the left panel of Figure 2. Note that the J_z calculated from our 3D geometrical model is significantly larger than the $J_{z,\rm ME}$, however both are clearly above the calculated uncertainties. The ME inversion delivers the magnetic field just at an average optical depth around $\log\tau = -1.5$ (Ruiz Cobo & del Toro Iniesta 1994). As we have seen before, larger electrical currents appear at the borders of structures with lower magnetic field and smaller optical depth. Consequently, the ME inversion probes higher layers above these structures resulting in a smaller derivative of the magnetic field than the one obtained from the 3D geometrical model. In the middle and right panels of Figure 2, we present the histograms of $J_{\rm hor}$ and J, respectively. In red, we show again the estimated uncertainties. As mentioned before, in most observational studies of electrical currents in solar active regions only the vertical component has been measured. We find $J_{\rm hor}$ to be about four times larger than J_z. Note that the horizontal component is clearly predominant, with a distribution practically equal to the one of J. Works estimating $J_{\rm hor}$ by making certain hypotheses on the $\vec{B}$ configuration reach similar results: Pevtsov & Peregud (1990) and Georgoulis & LaBonte (2004) found $J_{\rm hor} \sim 2$–3 times larger than J_z, while Ji et al. (2003) report on $J_{\rm hor}$ values of about one or two orders of magnitude larger than J_z. All studies estimating only J_z strongly underestimate $\vec{J}$ present in sunspot penumbrae.

Table 1 summarizes the values of $\langle|\ J_z\ |\rangle$, $\langle J_{\rm hor}\rangle$, and $\langle J\rangle$ at three different heights. The errors given in the table have been calculated by an error propagation from the distribution of $\vec{J}_{\rm err}$ described above. The electrical current density decreases with height and at all layers the horizontal component is on average about four times larger than the vertical one. While $\langle J_{\rm hor}\rangle$ decreases by 32% between the 0 and 200 km level, $\langle|\ J_z\ |\rangle$ shows a small decrease with height of about 17%. The large uncertainties at the 0 km level stem from the corresponding

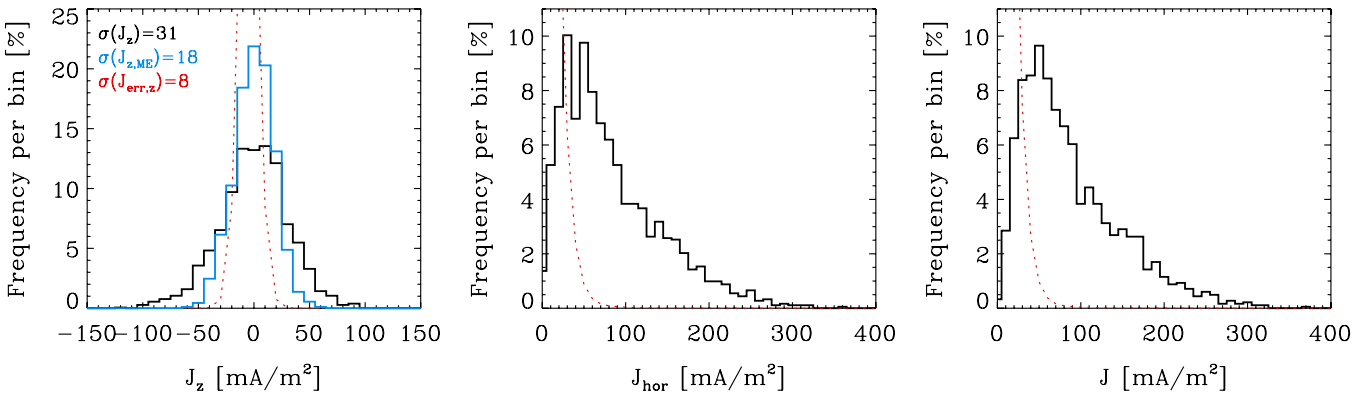

Figure 2. Left panel: histogram of J_z at 200 km (black) and histogram of J_z retrieved from a Milne–Eddington inversion (blue). Middle and right panels: histograms of $J_{\rm hor}$ and J evaluated at the same height layer. The red lines represent the corresponding error distributions.

Table 1
Mean Values of the Moduli of the Vertical and Horizontal Components of $\vec{J}$ as well as the Mean Value of J at Three Different Height Layers

z (km)	$\langle \mid J_z \mid \rangle$ (mA m^{-2})	$\langle J_{\rm hor} \rangle$ (mA m^{-2})	$\langle J \rangle$ (mA m^{-2})
0	30 ± 20	129 ± 50	135 ± 59
100	26 ± 9	103 ± 36	109 ± 39
200	25 ± 8	88 ± 33	93 ± 35
ME	15		

uncertainties of the determination of the magnetic field due to the low sensitivity of the visible lines used in this study.

The upper left panel of Figure 3 shows the histogram of the angle ψ formed by $\vec{B}$ and $\vec{J}$ at the 0 km height layer (black). In a force-free configuration, $\vec{B}$ and $\vec{J}$ are parallel to each other. In our volume, ψ is of about 20°. Since the uncertainty of ψ is large for pixels with small J, we also show the histogram of ψ for pixels with $J(z = 200) > 120$ mA m^{-2} (red line). The difference in the orientation of $\vec{B}$ and $\vec{J}$ is mainly due to a difference in their inclination from the vertical γ and not due to a difference in their azimuth ϕ as the upper right and lower left panels of Figure 3 indicate: both vector fields are basically in the same vertical plane. Consequently, the horizontal component of the Lorentz force must be larger than the vertical one. In fact, $\langle (\vec{J} \times \vec{B})_{\rm hor} \rangle$ amounts to 1.03 mdyn cm^{-3}, whereas $\langle (\vec{J} \times \vec{B})_z \rangle$ shows a value of 0.61 mdyn cm^{-3} only, both evaluated at $z = 0$ km for pixels with $J(z = 200) > 120$ mA m^{-2}. This is in agreement with Pevtsov & Peregud (1990), who also found the horizontal component of the Lorentz force being larger than the vertical one.

The lower right panel of Figure 3 shows the histograms of the energy dissipated by the electrical currents (ohmic energy) in the region under study integrated between the 0 and 200 km level (black). The ohmic energy has been calculated using the longitudinal electrical conductivity following Kopecký & Kuklin (1969) and is negligible in the inner sunspot penumbra compared with the solar flux. The energy is dissipated only at the borders of the horizontal tubes, where J reaches significant values (red line). In Paper I, we found that the main contribution to the energy flux carried by the ascending mass (convective energy) stems from layers below −75 km. The resulting convective energy flux, integrated from −225 to 200 km, reaches values of up to 78% of the solar flux, and thus would be sufficient to explain the observed penumbral brightness. However,

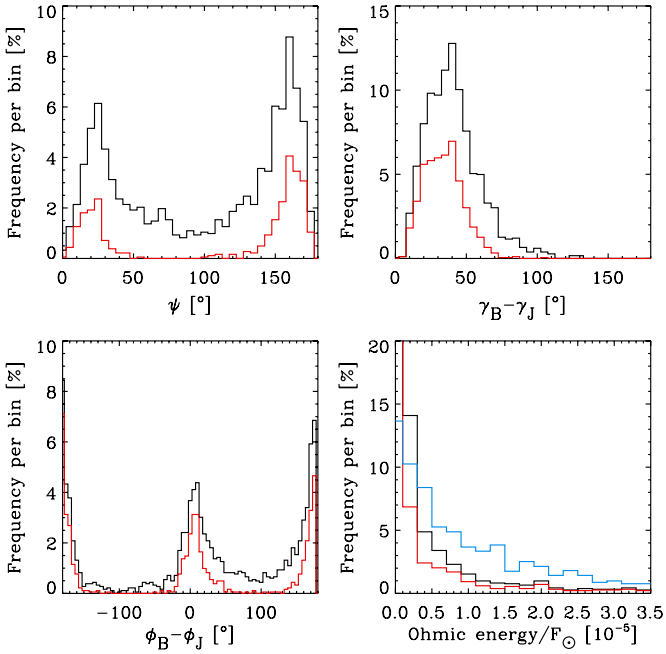

Figure 3. Upper left panel: histogram of the angle ψ between $\vec{J}$ and $\vec{B}$ at $z = 0$ km. Upper right panel: histogram of the difference between the inclination from the vertical of $\vec{B}$ and $\vec{J}$ at $z = 0$ km. Lower left panel: the same for the difference in azimuth. Lower right panel: energy dissipated by electrical currents in units of 10^{-5} solar flux (between 0 and 200 km, black, between −225 and 200 km, blue). In all the panels, the red line corresponds to angles and energies evaluated for those pixels with $J(z = 200) > 120$ mA m^{-2}.

this result has to be taken with care since the physical parameters at layers below −75 km entering this calculation result from extrapolations. If all the layers between −225 and 200 km are included in the calculation of the ohmic energy, the resulting values (well below 10^{-4} $F_\odot$) are still negligible for the energy balance (blue line in Figure 3).

The plasma β, defined as the ratio between the gas pressure and the magnetic pressure, is an important parameter to study the relevance of the Lorentz force in the dynamics of sunspot penumbrae. Figure 4 shows the plasma β at a height of 0 km. In our inner penumbral area, the $\beta = 1$ surface is strongly corrugated. Note that in the intraspines (areas enclosed by white contour lines) the plasma β is clearly larger than 1, being one order of magnitude lower in the spines. At the top layer (200 km) not presented here, the aspect is similar, although all values have decreased by a factor of ∼5.

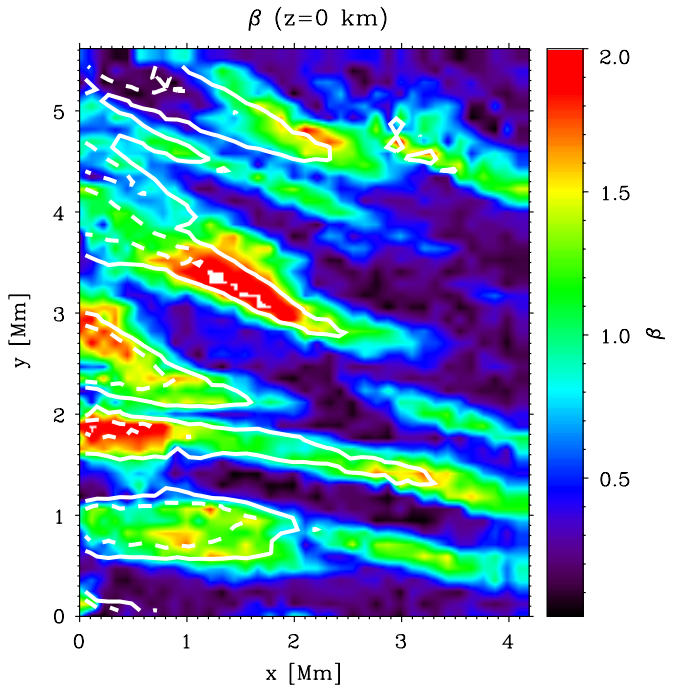

Figure 4. Map of the plasma β at $z = 0$ km. The contour lines correspond to B_z equal to -650 G (solid lines) and to -450 G (dashed lines).

3. CONCLUSIONS

The application of a genetic algorithm on the optical depth model retrieved from an SIR inversion of spectropolarimetric *Hinode*/SP data allowed us to construct a 3D geometrical model of a section of the inner penumbra of a sunspot (see Paper I). The resulting model has, by construction, a minimal divergence of $\vec{B}$ and a minimal deviation of the static equilibrium. This allows for the first time the accurate determination of the entire 3D electrical current density vector. At the 0.″32 resolution of the *Hinode*/SP, the electrical current density appears to be spatially resolved in the penumbra: significant J values (larger than 120 mA m^{-2}) are located at the borders of the intraspines. The electrical currents seem to wrap around the nearly horizontal flux tubes.

We find a horizontal component of $\vec{J}$ about four times larger than the vertical one. This is in agreement with earlier works estimating $J_{\rm hor}$ by assuming simplifying hypotheses on the $\vec{B}$ distribution. All works[3] only evaluating J_z clearly underestimate $\vec{J}$.

The magnetic field at lower layers is not force-free at the borders of the intraspines: there, the angle formed by $\vec{B}$ and $\vec{J}$ is about 20°. The difference in the orientation of $\vec{B}$ and $\vec{J}$ is mainly due to a different inclination with respect to the vertical of both vectors, being nearly negligible the difference in azimuth, leading to a dominant horizontal component of the Lorentz force, directed toward the central axis of the intraspines, something that helps them to maintain the internal force balance. At the 0 km level, the plasma β is strongly corrugated, being larger than 1 at the borders and inside the intraspines and one order of magnitude lower inside the spines. In the latter, the Lorentz force can hardly be balanced by the pressure gradient or weight of the material: consequently the magnetic field configuration of the spines in the inner penumbra must be close to a force-free configuration. Furthermore, as in these areas J is relatively small and B is large, the field must be closer to being potential. Following the same reasoning, our results show that at the highest layers the plasma β is nearly everywhere below 0.3 and thus the field must be closer to a force-free configuration almost everywhere and to a potential one in the spines.

The dissipated ohmic energy is clearly negligible being five orders of magnitudes smaller than the solar flux.

This work has been supported by the Spanish Ministerio de Ciencia e Innovación through projects ESP 2006-13030-C06-01, AYA2007-65602, AYA2009-14105-C06-03, AYA2007-63881, and the European Commission through the SOLAIRE Network (MTRN-CT-2006-035484). We thank C. Beck for fruitful discussion.

[3] Except Venkatakrishnan & Tiwari (2009): they find J_z values in the range of GA m^{-2}, certainly a slip of their units.

REFERENCES

Balthasar, H. 2006, A&A, 449, 1169
Balthasar, H., & Gömöry, P. 2008, A&A, 488, 1085
Borrero, J. M., & Solanki, S. K. 2010, ApJ, 709, 349
Canfield, R. C., et al. 1992, PASJ, 44, L111
de la Beaujardiere, J. F., Canfield, R. C., & Leka, K. D. 1993, ApJ, 411, 378
Deloach, A. C., Hagyard, M. J., Rabin, D., Moore, R. L., Smith, B. J., West, E. A., & Tandberg-Hanssen, E. 1984, Sol. Phys., 91, 235
Gao, Y., Xu, H., & Zhang, H. 2008, Adv. Space Res., 42, 888
Gary, G. A., & Demoulin, P. 1995, ApJ, 445, 982
Georgoulis, M. K., & LaBonte, B. J. 2004, ApJ, 615, 1029
Hagyard, M. J. 1988, Sol. Phys., 115, 107
Hofmann, A., Grigorjev, V. M., & Selivanov, V. L. 1988, Astron. Nachr., 309, 373
Hofmann, A., Ruzdjak, V., & Vrsnak, B. 1989, Hvar Obs. Bull., 13, 11
Ji, H. S., Song, M. T., Zhang, Y. A., & Song, S. M. 2003, Chin. Astron. Astrophys., 27, 79
Jurcák, J., Martínez Pillet, V., & Sobotka, M. 2006, A&A, 453, 1079
Kopecký, M., & Kuklin, G. V. 1969, Sol. Phys., 6, 241
Lagg, A., Woch, J., Krupp, N., & Solanki, S. K. 2004, A&A, 414, 1109
Leka, K. D., Canfield, R. C., McClymont, A. N., de La Beaujardiere, J.-F., Fan, Y., & Tang, F. 1993, ApJ, 411, 370
Li, J., Metcalf, T. R., Canfield, R. C., Wuelser, J.-P., & Kosugi, T. 1997, ApJ, 482, 490
Li, J., van Ballegooijen, A. A., & Mickey, D. 2009, ApJ, 692, 1543
Lites, B. W., Elmore, D. F., Seagraves, P., & Skumanich, A. 1993, ApJ, 418, 928
Martínez Pillet, V. 2000, A&A, 361, 734
Metcalf, T. R., Canfield, R. C., Hudson, H. S., Mickey, D. L., Wulser, J.-P., Martens, P. C. H., & Tsuneta, S. 1994, ApJ, 428, 860
Pevtsov, A. A., & Peregud, N. L. 1990, in Physics of Magnetic Flux Ropes, ed. C. T. Russell, E. R. Priest, & L. C. Lee (Washington, DC: American Geophysical Union), 161
Puschmann, K. G., Ruiz Cobo, B., Vázquez, M., Bonet, J. A., & Hanslmaier, A. 2005, A&A, 441, 1157
Puschmann, K. G., Ruiz Cobo, R., & Martínez Pillet, V. 2010, ApJ, 720, 1417 (Paper I)
Ruiz Cobo, B., & del Toro Iniesta, J. C. 1992, ApJ, 398, 375
Ruiz Cobo, B., & del Toro Iniesta, J. C. 1994, A&A, 283, 129
Sánchez Almeida, J. 2005, ApJ, 622, 1292
Schlichenmaier, R., Jahn, K., & Schmidt, H. U. 1998a, A&A, 337, 897
Schlichenmaier, R., Jahn, K., & Schmidt, H. U. 1998b, ApJ, 493, 121
Shimizu, T., et al. 2009, ApJ, 696, L66
Skumanich, A., & Lites, B. W. 1987, ApJ, 322, 473
Socas-Navarro, H. 2005, ApJ, 633, L57
Solanki, S. K., & Montavon, C. A. P. 1993, A&A, 275, 283
van Driel-Gesztelyi, L., Hofmann, A., Demoulin, P., Schmieder, B., & Csepura, G. 1994, Sol. Phys., 149, 309
Venkatakrishnan, P., & Tiwari, S. K. 2009, ApJ, 706, L114
Wang, T., Xu, A., & Zhang, H. 1994, Sol. Phys., 155, 99
Zhang, H., & Wang, T. 1994, Sol. Phys., 151, 129